Pakistan Veterinary Journal

ISSN: 0253-8318 (PRINT), 2074-7764 (ONLINE)
DOI: 10.29261/pakvetj/2025.150

RESEARCH ARTICLE

Morphological and Mitochondrial Genome Characterization of *Hypoderma Sinense*: Insights into Evolutionary Relationships Within Oestridae

Bin Shi[1,2], Xia-Ling Zhao[2#], Wen-Qiang Tang[2], Fu-Bin Gan[3], Yan-Bin Li[4], Fu-Qiang Huang[4], Danqulamu[2], Ming Qi[3], Ming-Zhu Zhang[5], Xiao-Ya Li[3], Hai-Long Dong[1], Munwar Ali[6], Ahmed A. El-Mansi[7], Abdelalim A. Gadallah[8], Kun Li[6] and Qing-Xia Wu[1*]

[1]Xizang Agricultural and Animal Husbandry University, Linzhi 860000. China; [2]Institute of Animal Science, Tibet Academy of Agricultural and Animal Husbandry Sciences, Lhasa 850009, China; [3]Nyingchi Agricultural and Rural Affairs Bureau, Linzhi 860000, China; [4]College of Animal Science and Technology, Foshan University, Foshan 528225, China; [5]Lhasa of transcribing district bureau of agriculture and rural areas, Lhasa 850100, China; [6]College of Veterinary Medicine, Nanjing Agricultural University, Nanjing 210095, China; [7]Biology Department, Faculty of Science, King Khalid University, Abha 61413, Saudi Arabia; [8]Biology Department, College of Science, Jazan University, Jazan, Kingdom of Saudi Arabia. [#]Co-first author with equal contribution.
*Corresponding author: goodwqx@163.com

ARTICLE HISTORY (25-180)

Received: February 27- 2025
Revised: April 9, 2025
Accepted: April 10, 2025
Published online: April 21, 2025

Key words:
Hypoderma sinense
Mitochondrial genome
Oestridae
Phylogenetic relationships

ABSTRACT

In mammals, the *Hypoderma* flies and their larvae are obligate parasites causing cutaneous myiasis. *Hypoderma (H.) sinense* of this genus mainly parasitizes yaks and cattle. With an eye towards unique morphological traits for correct identification and differentiation within the family Oestridae, this work investigated third-stage larvae of *H. sinense* under a stereomicroscope and scanning electron microscopy. The key elements analyzed were segmentation, the cephalic segment structure, spiracular plates, the ventral side, and spines. Moreover, the mitochondrial (mt) genome of *H. sinense* was recovered from enriched mt samples with conventional molecular methods. The complete sequence of 16,296bp was obtained using next-generation sequencing (NGS). Around 13 protein-coding genes (PCGs), 22 transfer RNA genes, two ribosomal RNA genes, and a non-coding section were identified using bioinformatic methods for genome annotations. Using the 13 PCGs, the phylogenetic study evaluated the Oestridae family evolutionary relationships between *H. sinense* and related species. With 40.50% A, 36.75% T, 14.41% C, and 8.34% G, the *H. sinense* mt genome had an A+T content of 77.25%, far higher than the G+C content. Phylogenetic studies based on the 13 PCGs showed that *H. sinense* developed a monophyletic clade including *H. lineatum*, *H. bovis*, and *H. pantholopsum*. This work reveals the first complete mt genome of *H. sinense*, therefore offering vital molecular data that improves our knowledge of the Oestridae family phylogenetic ties.

To Cite This Article: Shi B, Zhao XL, Tang WQ, Gan FB, Li YB, Huang FQ, Danqulamu, Qi M, Zhang MZ, Li XY, Dong HL, Ali M, El-Mansi AA, Gadallah AA, Li K and Wu QX, 2025. Morphological and Mitochondrial Genome Characterization of *Hypoderma Sinense:* Insights into Evolutionary Relationships Within Oestridae. Pak Vet J, 45(2): 767-774. http://dx.doi.org/10.29261/pakvetj/2025.150

INTRODUCTION

Third-stage larvae of flies in the genus *Hypoderma (H.)* are in charge of creating hypodermosis, which belongs to the Oestridae family, and the Diptera order (Colwell and Otranto, 2021; González *et al.*, 2024). Cutaneous myiasis, or cutaneous myiasis results from these larvae invading the subcutaneous tissues of several mammalian hosts (Sunny *et al.*, 2016; González *et al.*, 2023). All of these disorders, in spontaneous abortion, lowered breastfeeding, weight loss, and impaired reproductive capacity, contribute to notable economic losses in the cattle sector (Otranto *et al.*, 2005). The species of *Hypoderma*, including *H. bovis* and *H. lineatum* in bovines (Patra *et al.*, 2018), *H. diana* (Kettle and Utsi, 1955), *H. actaeon* and *H. tarandi* in Cervidae (Ahmed *et al.*, 2017a), *H. sinense* (Otranto *et al.*, 2005), and *H. pantholopsum* (Zhang *et al.*, 2025) in yaks, antelopes, and cattle (Xiuping Li *et al.*, 2020), are relatively well-defined (Chen *et al.*, 2024). Among these, *H. sinense* is indigenous to the Qinghai-Tibet Plateau in China, where hypodermosis

brought on by *H. sinense* is the most important arthropod illness in the area (Ruan *et al.*, 2014). Although rare infestations of other animals, including sheep, horses, and deer, these flies mostly parasitize yaks and cattle (Otranto *et al.*, 2016; Shaalan *et al.*, 2024). Additionally, possible for human infection to occur with these parasites (Bernhardt *et al.*, 2019). Significant financial losses in the cattle sector are caused by this zoonotic parasite disease (Otranto *et al.*, 2005). Pastured on the Tibetan plateau, yaks have a range in myiasis incidence from 70% to 80%; rates in some regions approach 100% (Otranto *et al.*, 2006). The Tibetan people mostly rely on yaks for their revenue; hence, precise identification of the fly species is crucial for reducing hypodermosis. Usually found by morphological characteristics seen under a stereomicroscope, the third-stage larvae of these flies can be difficult to distinguish amongst members of the Oestridae family. Some related species' taxonomy has long been divisive (Otranto *et al.*, 2006; Cameron, 2014), and the precise identification and differentiation of this species depend on a thorough understanding of the morphology and genetic sequences of *H. sinense*, which is yet lacking. Of great interest for phylogenetic and genetic pedigree study, the mitochondrial genome (mt) has a straightforward structure, low molecular weight, and greater emergence rate than the nuclear genome (Bentler, 2010). Next-generation sequencing (NGS) technology emerged and resulted in the sequencing and annotation of ever more Oestridae mt genomes. Up till June 2024, the NCBI RefSeq database had 21 whole mt genomes of Oestridae, and the NCBI GenBank database had five whole mt genomes of *Hypoderma*, one of which was obtained in the given research (Accession: NC_071819). The absence of a complete mitochondrial genome for *H. sinense* has impeded precise phylogenetic resolution and evolutionary comparisons within Hypodermatinae. Therefore, this study identified *H. sinense* using scanning electron microscopy. Its molecular taxonomy for further identification, sequencing, and annotation of its complete mt genome was carried out by applying NGS technology. By using protein-coding genes (PCGs) of the mt genome, a phylogenetic tree was constructed, and the evolutionary relationships between *H. sinense* and other Oestridae, specifically within the Hypodermatinae, were discussed.

MATERIALS AND METHODS

Ethical approval: The study was approved by the Animal Welfare Committee of Nanjing Agricultural University on the Ethics of Animal Care (NJAU.No.20230413054).

Identification of *H. sinense:* Cutaneous samples of *H. sinense* were collected from yaks in Gongbujiangda County, Nyingchi City, Tibet, and were identified using a Leica SAPO stereo microscope. Pictorial views of the Oestridaes were gained with a microscope camera (MC170 HD). Additionally, a scanning electron microscope, known for its high magnification capabilities, was used to reveal the morphological characteristics of the three-dimensional structure of the sample surface, making it an effective method for identifying.

DNA extraction and sequencing: Using tissue grinding pestles, individual *H. sinense* specimens were ground, and total DNA extraction was performed by silica gel column chromatography through the FastPure Tissue/Cell/Bacteria/Blood DNA Isolation Kit following the manufacturer's instructions (Nanjing Vazyme Biotech Co., Ltd, Cat. DC112–01). The complete genome shotgun (WGS) technique using next-generation sequencing (NGS) was applied at Shanghai Personal Biotechnology Co., Ltd. Sequencing was done on the Illumina NovaSeq platform (Illumina, San Diego, CA, USA) in 2×150bp paired-end mode. The data obtained in raw form after genomic sequencing were then subjected to a computer-based system for characterization and analysis of the genome. To verify the quality of resultant data, FastQC software was used, and low-quality 3′-end reads were removed by the Adapter Removal (version 2) program (Schubert *et al.*, 2016). For validation of the NGS results, PCR was performed using extracted DNA to amplify the nad1 gene, which was subsequently sequenced by Sanger sequencing. To perform PCRs, a Taq PCR Master Mix Kit (Sangon Biotech, China) in a thermal cycler (Biometra TAdvanced 96 SG, Germany) was utilized. A segment of mt DNA (~1350bp) was amplified by using HLLeuR (5'-CTATTTTGGCAGATTAGTGCAATAAAT-3') and cytbF (5'-CTGTAATTTTATTAACTTGAATTGGAGC-3') primers.

Assembly and annotation of the mitochondrial genome: Assembly of high-quality NGS data was performed using A5-miseq v20150522 (Coil *et al.*, 2014) and SPAdesv3.9.0 (Bankevich *et al.*, 2012), leading to the construction of contig and scaffold sequences. Mitogenome sequences from each assembly were analyzed through BLASTN searches against the NCBI nt database (BLAST v2.2.31+) using sequences with high read coverage as queries. The analysis employed default parameters to identify homologous regions for sequence alignment and statistical evaluation (Altschul *et al.*, 1990). Collinearity analysis was performed using MUMmer v3.1 software to ascertain the linkages in terms of position between contigs and therefore enable gap filling through a reference sequence (Kurtz *et al.*, 2004). Pilon v1.18 (Walker *et al.*, 2014) helped us to get the last corrected mt sequence.

MITOS was used to verify the whole mt genome sequence of *H. sinense* for baseline labelling and RNA gene secondary structure prediction (Bernt *et al.*, 2013). Furthermore, supporting the results were homology investigations compatible with other trematode species. This was carried out on top of the hand editing of the annotated data done with SnapGene (version 6.0.2). With the CGView Server (Grant and Stothard, 2008), we looked at and found the structure of the mitogenome and the GC skew. PhyloSuite was used (Zhang *et al.*, 2020) to estimate relative synonymous codon usage (RSCU) and composition skew. Conversely, UniPro UGENE (Okonechnikov *et al.*, 2012) was used to run the computations.

Phylogenetic assessment: Two species of Hippoboscoidea and fifty species of Oestroidea had mt genome sequences obtained for comparison and phylogenetic study. Then PhyloSuite helped 13 protein-coding genes (PCGs) recover from 52 mt genomic sequences. First, normalizing the sequences using both manual and PhyloSuite approaches helped to verify whether names and annotations are

accurate. The MAFFT program was applied to align the PCGs (Katoh and Standley, 2016). Following the removal of poorly aligned areas with Gblocks 0.91b (Talavera and Castresana, 2007), PhyloSuite helped to compile a single dataset from the aligned PCGs. Later, the resulting files were investigated using PartitionFinder2 (Lanfear *et al.*, 2017) to identify the most preferred phylogenetic frame for every gene; this information was then used in MrBayes (Ronquist *et al.*, 2012) for phylogenetic studies. By use of a partitioned model (Chernomor *et al.*2016) of nucleotide substitution and ultrafast bootstrap values (Wang *et al.*, 2018), the tree was built using 100,000 replicates. At last, iTOL v5 (Letunic and Bork, 2021) was used for visualisation and annotation of produced phylograms.

RESULTS

Morphological characteristics: Microscopic studies found that the third-stage larvae of *H. sinense* comprised eleven components: one cephalic, two thoracic, and eight abdominal portions with an inward ventral side. Additionally, a transverse fissure extended from the posterior end of the pseudo-head to the middle of the belly, accompanied by two smaller fleshy protrusions on the posterior side. Present on the ventral side, spines stretched from the first thoracic segment to the abdominal segments in six clusters (Fig. 1).

Using scanning electron microscopy, *H. sinense* was distinguished from other Oestridae by specific morphological traits. Notably, there was a pair of thick spiracular plates at the posterior end, featuring evident gaps in the C-ring plane. The ecdysal scar protruded at the center of the spiracular plate, which contains numerous spiracular openings and a limited number of spines (Fig. 2 and 3).

Mitogenome structure and nucleotide composition: Through gap sequencing, gene splicing, and assembly, the complete mt genome sequence of *H. sinense* was determined to be 16,296 bp in length (GenBank accession: NC_071819). The genome contained the following share of bases: A - 40.50 %, T - 36.75 %, C - 14.41 %, and G - 8.34 %, indicating a prominent AT bias. Additionally, GC and AT skew values were 0.267 and 0.049, respectively (Table 1).

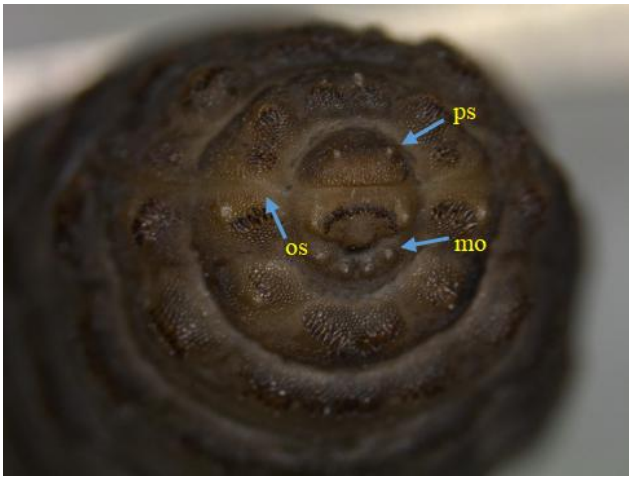

Fig. 1: Morphology of the cephalic segment of *H. sinense* from Tibet. Arrow indicates the os: pseudocephalon, mo: mouth opening, and os: opercular scar, respectively.

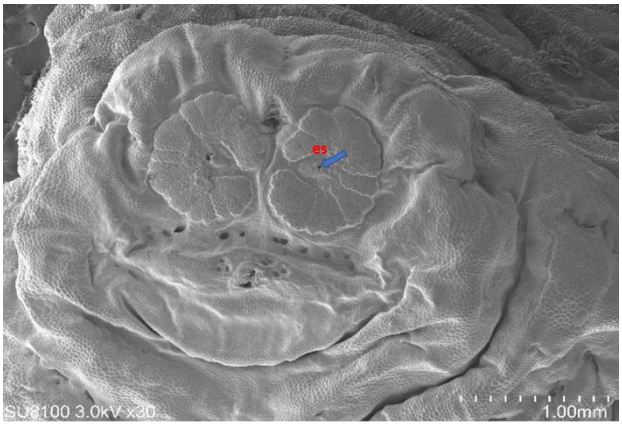

Fig. 2: Scanning electron micrograph of the spiracular plates of *H. sinense* from Tibet. The arrow indicates the ecdysal scar of the spiracular plate. es: ecdysal scar, Scale bar=1.00 mm.

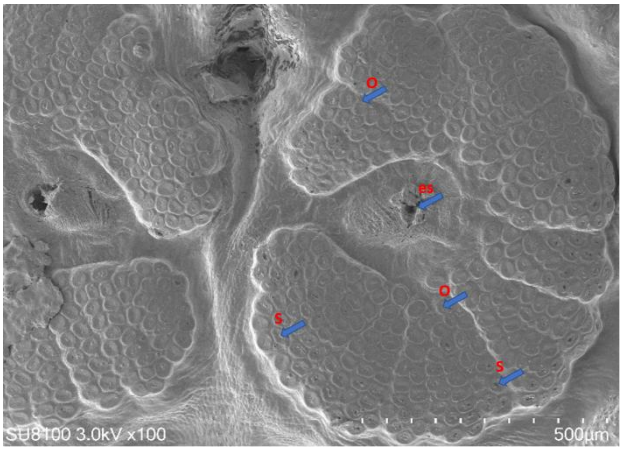

Fig. 3: Scanning electron micrograph of surfaces of the spiracular plates of *H. sinense* from Tibet. O: spiracular opening, S: spine, es: ecdysal scar, Scale bar=500 µm.

After genome annotation, it was clarified that the mt genome in total has 36 genes, including 13 genes responsible for protein-coding (PC), 2 rRNA, and 22 tRNA genes, along with a non-coding region. The total length of the 13 PCGs was 11,295 bp, with an A + T content of 75.1 %. The combined length of 22 tRNA gene sequences was 1,450bp, with an A + T content of 77.7 %. The two rRNA genes had a total length of 2,107 bp, with an A + T content of 80.2% (Table 2). The mt genome of *H. sinense* included 15 gene spacers, a 1 to 87bp length range. In addition to that, 17 overlapped genes were detected with sizes varying from 1 to 77bp (Table 2).

Codon usage and protein-coding genes: Among the genes responsible for protein-coding genes, the *nad5* gene was the longest, measuring 1,758bp (nucleotide positions 6,266-8,023), followed by the *cox1* gene, which measured 1,527bp (positions 1,414-2,940). The shortest gene, *Atp8*, was 165bp long (positions 3,826-3,990). The *nad2* and *atp8* genes had ATT as the start codon, while ATG was the start codon in the sequences of *cox3*, *cox2*, *atp6*, *nad4*, *cob*, and *nad4l* genes. The *cox1*, *nad1*, *nad3*, and *nad6* genes began with ATA, with only one PCG starting with ATC. The primary stop codon in the sequences of PCGs was TAA, while three PCGs ended with TAG. Of the 13 PCGs of *H. sinense*, 9 genes (*nad2*, *cox1*, *cox2*, *atp8*,

Table 1: Lengths and arrangement of genes in the mitochondrial genome of *H. sinense*

Feature	Strand	Position	Length (bp)	Initiation codon	Stop codon	Anticodon	Intergenic nucleotide
trnI	N	1-64	64			GAT	-3
trnQ	J	62-130	69			TTG	-1
trnM	N	130-197	68			CAT	
nad2	N	198-1,214	1017	ATT	TAA		-2
TrnW	N	1,213-1,280	68			TCA	-8
trnC	J	1,273-1,335	63			GCA	3
trnY	J	1,339-1,403	65			GTA	10
cox1	N	1,414-2,940	1527	ATA	TAA		-5
trnL2	N	2,936-3,001	66			TAA	4
cox2	N	3,006-3,686	681	ATG	TAA		3
trnK	N	3,690-3,760	71			CTT	-1
trnD	N	3,760-3,825	66			GTC	
atp8	N	3,826-3,990	165	ATT	TAA		-7
atp6	N	3,984-4,661	678	ATG	TAA		-1
cox3	N	4,661-5,449	789	ATG	TAA		6
trnG	N	5,456-5,520	65			TCC	-3
nad3	N	5,518-5,874	357	ATA	TAA		-1
trnA	N	5,874-5,937	64			TGC	5
trnR	N	5,943-6,004	62			TCG	
trnN	N	6,005-6,068	64			GTT	
trnS1	N	6,069-6,136	68			GCT	2
trnE	N	6.139-6,203	65			TTC	17
trnF	J	6,221-6,285	65			GAA	-20
nad5	J	6,266-8,023	1758	ATC	TAG		-3
trnH	J	8,021-8,085	65			GTG	1
nad4	J	8,087-9,427	1341	ATG	TAG		-7
nad41	J	9,421-9,711	291	ATG	TAA		2
trnT	N	9,714-9,778	65			TGT	
trnP	J	9,779-9,843	65			TGG	-88
nad6	N	9,756-10,370	615	ATA	TAA		-1
cob	N	10,370-11,506	1137	ATG	TAG		-2
trnS2	N	11,505-11,571	67			TGA	68
nad1	J	11,640-12,578	939	ATA	TAA		10
trnL1	J	12,589-12,651	63			TAG	-23
rrnL	J	12,629-13,945	1317				28
trnV	J	13,974-14,045	72			TAC	-2
rrnS	J	14.044-14.833	790				1076
OH	N	15,910-16.044	135				251

Table 2: Base composition of the complete mitochondrial genome, protein-coding genes, and rRNA genes of H. sinense

Regions	Strand	Size (bp)	T(U) (%)	C (%)	A (%)	G (%)	AT (%)	GC (%)	GT (%)	AT skewness	GC skewness
Full genome	+	16296	36.75	14.41	40.5	8.34	77.25	22.75	45.09	0.049	-0.267
PCGs	all	11295	42.9	12.4	32.2	12.4	75.1	24.9	55.3	-0.142	0
PCGs	+	6966	39.8	15.6	34.2	10.5	74	26.1	50.3	-0.076	-0.195
PCGs	-	4329	48.0	7.3	29	15.6	77	22.9	63.6	-0.248	0.362
tRNAs	all	1450	37.7	9.8	40	12.5	77.7	22.3	50.2	0.03	0.121
tRNAs	+	923	36.6	11.4	40.6	11.4	77.2	22.8	48	0.052	0
tRNAs	-	527	39.7	7.0	38.9	14.4	78.6	21.4	54.1	-0.01	0.346
rRNAs	all	2,107	41.7	6.4	38.5	13.4	80.2	19.8	55.1	-0.04	0.354
rRNAs	-	2,107	41.7	6.4	38.5	13.4	80.2	19.8	55.1	-0.04	0.354
atp6	+	678	40.56	15.19	34.81	9.44	75.37	24.63	50	-0.076	-0.234
atp8	+	165	40.61	12.12	43.64	3.64	84.24	15.76	44.25	0.036	-0.538
cox1	+	1527	37.79	16.04	31.83	14.34	69.61	30.39	52.13	-0.086	-0.056
cox2	+	681	36.86	17.62	33.77	11.75	70.63	29.37	48.61	-0.044	-0.2
cox3	+	789	38.53	17.74	30.42	13.31	68.95	31.05	51.84	-0.118	-0.143
cob	+	1137	39.31	15.74	34.04	10.91	73.35	26.65	50.22	-0.072	-0.182
nad1	-	939	49.09	7.45	25.99	17.47	75.08	24.92	66.56	-0.308	0.402
nad2	+	1017	42.97	13.37	36.58	7.08	79.55	20.45	50.05	-0.08	-0.308
nad3	+	357	43.42	17.37	32.77	6.44	76.19	23.81	49.86	-0.14	-0.459
nad4	-	1341	47.95	6.94	29.16	15.96	77.11	22.89	63.91	-0.244	0.394
nad4L	-	291	49.48	5.15	29.9	15.46	79.38	20.62	64.94	-0.247	0.5
nad5	-	1758	47.33	7.79	30.43	14.45	77.76	22.24	61.78	-0.217	0.299
nad6	+	615	41.63	13.66	38.86	5.85	80.49	19.51	47.48	-0.034	-0.4
rrnL	-	1317	42.14	6.07	39.33	12.45	81.47	18.53	54.59	-0.034	0.344
rrnS	-	790	40.89	6.96	37.22	14.94	78.1	21.9	55.83	-0.047	0.364

+: sense strand (coding strand).

atp6, *cox3*, *nad3*, *nad6*, and *cob*) were encoded on the majority strand (J-strand), while 4 genes (*nad5*, *nad4*, *nad4L*, *nad1*) were encoded on the minority strand (N-strand) (Table 1). The codon usage, relative synonymous codon usage (RSCU), and codon family ratios are shown in Fig. 4. Isoleucine (9.77%), leucine (16.04%, comprising 3.15%+12.89%), and serine (9.77%, comprising 3.04%+6.73%) dominated among the PCGs of *H. sinense*. To verify the NGS outcomes and to check the structure of the *nad1* gene, a pair of primers was

designed to sequence its start and end parts. The results indicated that the *nad1* gene started at 11,640 bp and ended at 12,578 bp, encoding 270 amino acids (Fig. 5).

tRNA and rRNA genes: A total of 22 tRNA genes were detected in the mt genome of *H. sinense*, with sizes ranging from 62bp (*trnR*) to 72bp (*trnV*) (Table 1). MITOS predicted that most of the tRNA genes possessed a full cloverleaf configuration. A G-nucleotide was observed in the concatenated tRNA sequence in the mt genome of *H. sinense*, with a GC skew of 0.121. The lengths of the two rRNA genes, *rrnS* and *rrnL*, were 1,317bp and 790bp, respectively, with A+T base contents of 81.5% and 78.1%, respectively (Table 2). The two rRNA genes were separated by *trnV*. All 22 typical insect tRNA genes were distributed discontinuously throughout the mt genome (Table 1, Fig. 6).

Phylogenetic analysis: The genetic lineage was constructed to elucidate the phylogenetic relationships among the complete mt genes of *H. sinense* and other larvae in the Oestridae family. The analysis utilized 13 PCG datasets from 52 reported mt genomes accessible in the NCBI repository, with the sequences of *Melophagus ovinus* (NC_037368) and *Ornithomya biloba* (NC_061211) serving as outgroups. The phylogenetic tree analysis showed that 50 species from various families within Oestroidea, including Calliphoridae, Oestridae, Sarcophagidae, Rhiniidae, Polleniidae, and Tachinidae, were divided into two main clades. Clade I consisted of 9 species representing the subfamily Gasterophilinae, while clade II included 41 representatives from 12 subfamilies. Notably, Clade II contained *H. sinense*, *H. lineatum*, *H. bovis*, and *H. pantholopsum*, all from the subfamily Hypodermatinae within the genus *Hypoderma*. Furthermore, within the Oestroidea superfamily, the subfamily Hypodermatinae was found to be closely related to the Oestrinae and Cuterebrinae subfamilies of the Oestridae family (Fig. 7).

Fig. 4: The Relative Synonymous Codon Usage (RSCU) for the entire mitogenome of *H. sinense* is shown, with the codon families labeled along the x-axis. The values displayed at the top of each bar represent the amino acid frequency.

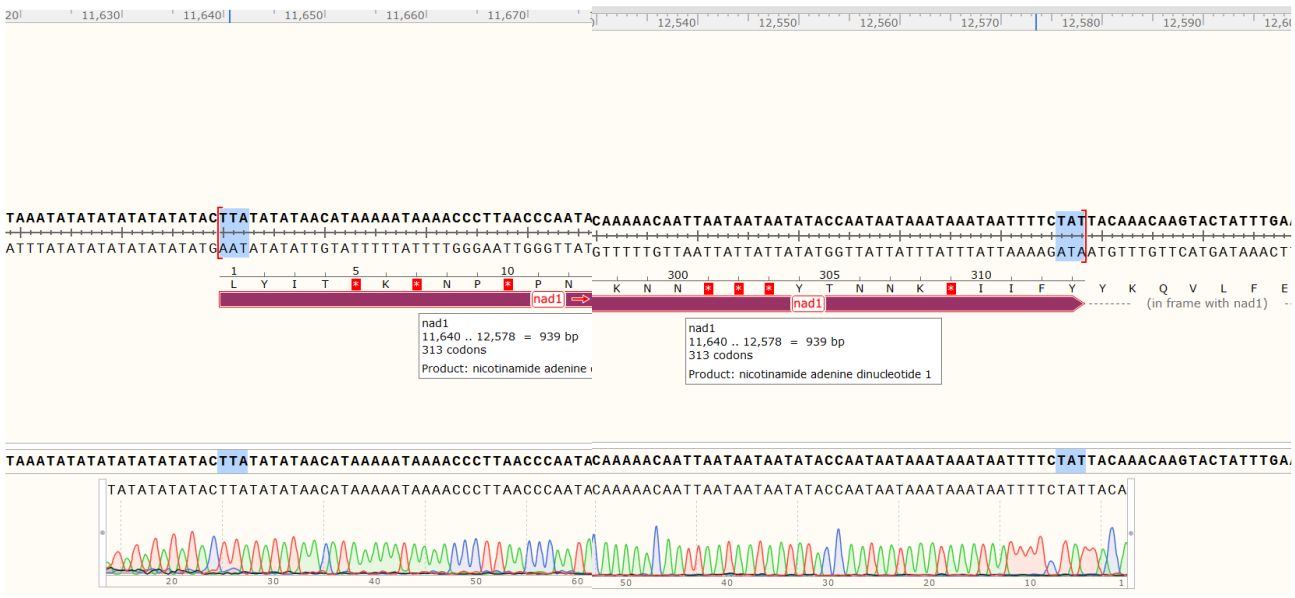

Fig. 5: Location and length of the nad1 gene in the mitogenome of *H. sinense*.

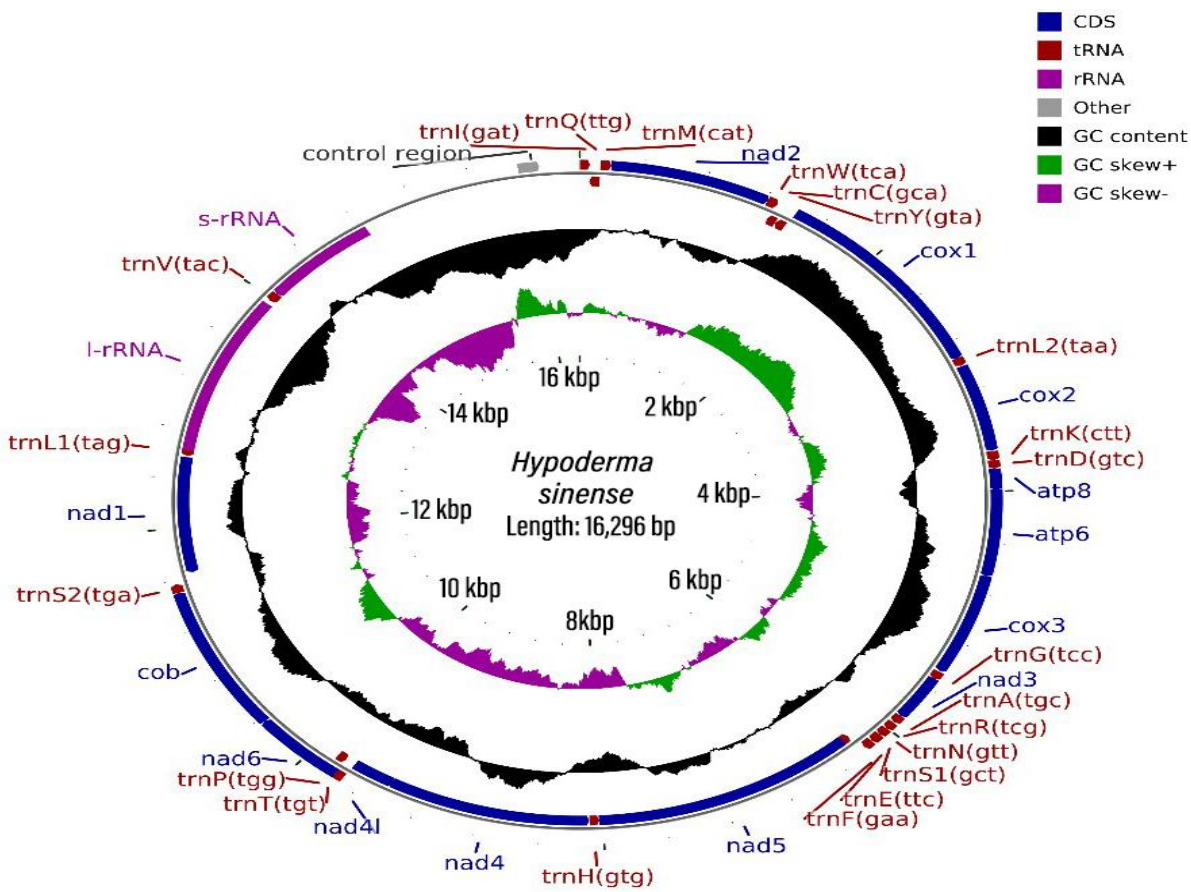

Fig. 6: Structure of the mitogenome of *H. sinense.*

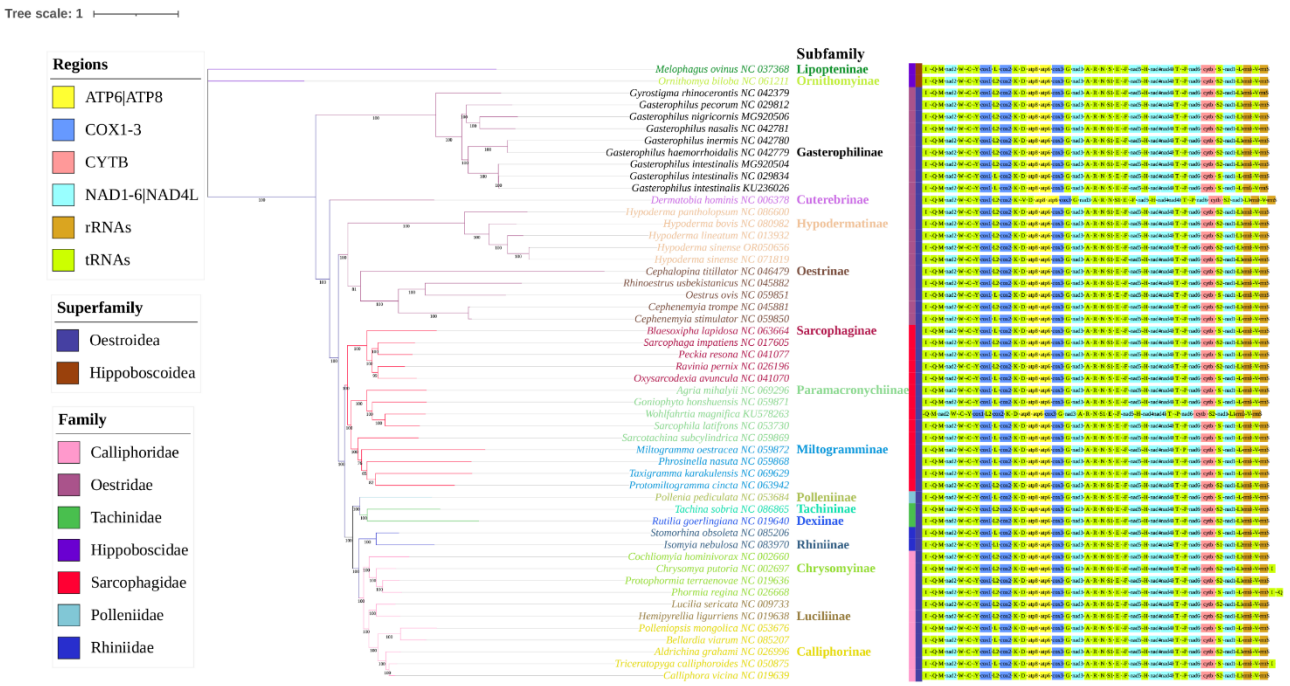

Fig. 7: Phylogenetic relationships between *H. sinense* and the Oestroidea superfamily based on mitochondrial sequences. The sequences of *Melophagus ovinus* (NC_037368) and *Ornithomya biloba* (NC_061211) serve as outgroups. A phylogenetic tree was generated using the MrBayes approach based on 13 protein-coding genes.

DISCUSSION

The third stage of *H. sinense* larvae is the most frequently retrieved stage by professionals and veterinarians from both intact and processed (slaughtered) animals, making morphological identification primarily based on this stage (L3). Key identification features of *H. sinense* include characteristics of the mouth opening, the ventral side of the tenth abdominal part, and the spiracular plates at the posterior end (Otranto *et al.*, 2003). In this

study, these key identification sites of *H. sinense* third-stage larvae were observed using a stereomicroscope and scanning electron microscope, and the findings were consistent with previous research (Ahmed *et al.,* 2017b; Otranto *et al.,* 2004). The larvae, for instance, have a bent ventral side and consist of eleven segments: one cephalic, two thoracic, and eight abdominal. Accompanying two fleshy protrusions, a transverse fissure stretched from the posterior pseudo-head to the abdomen. Six clusters of spines ran from the first thoracic to the abdominal segments. *H. sinense* differs from other Oestridae in several morphological features, including its thick spiracular plates, gaps in the C-ring plane, and a projecting ecdysal scar with several spiracular apertures.

In taxonomic categorization of organisms, the mt genome is rather important. Combining several genetic sequences has been found in studies to boost the dependability and stability of phylogenetic modelling (Nguyen *et al.,* 2015). Thus, in the given work, the full mt genome of *H. sinense* was ascertained and checked, producing an mt gene sequence of 16,296bp including 13 PCGs, two rRNAs, 22 tRNAs, and one non-coding region. There was A–40.50%, T–36.75%, C–14.41%, and G–8.34% in the base makeup. The mt genome of *H. sinense* was determined to be comparable to that of other bot flies of the genus *Hypoderma* (e.g., 16,283 bp for *H. bovis* [Accession: NC_080982.1], 16,354 bp for *H. lineatum* [Accession: NC_013932.1], and 16,265bp for *H. pantholopsum* [Accession: NC_086600.1]). All these genes followed the same sequence and orientation as those of primitive insect genomes (Boore, 1999). Common to most bot flies (Oestridae), the A+T base content was much higher than the G+C base content (Weigl *et al.,* 2010a). The start codon for PCGs in *H. sinense* differed from that of *H. lineatum*; previous research indicated that the start codon for *H. lineatum cox1* was TCG (Weigl *et al.,* 2010a), a nonstandard start codon also reported in some species of Calliphoridae (Lessinger *et al.,* 2000). Additionally, *H. lineatum* exhibited some PCGs having T stop codons (abbreviated); however, the mt genome of *H. sinense*, which was sequenced, did not show this phenomenon. Previous studies indicated that the *nad1* gene measured 939bp in *H. sinense*, *H. diana*, *H. bovis*, and *H. lineatum* (Weigl *et al.,* 2010b), which is consistent with the results of *H. sinense* in this study.

The taxonomy and classification of bot flies have been extensively debated (Li *et al.,* 2019), with divisions in different families. Past studies on Oestridae have been focused on its existence-related history and its percentage presence, but there is insufficient phylogenetic data available. Weigl *et al.* (2010b) analyzed the phylogeny of nad1 sequence data using the Kimura two-parameter model, while Rakhshandehroo *et al.* (2019) employed the maximum likelihood method to analyze the nucleotide sequence of the COI gene, yielding different results. Research has shown that mt genome sequences can offer valuable genetic markers for assessing the taxonomic status of flies, especially when PCG sequences are utilized for comparative analysis (de Azeredo-Espin and Lessinger, 2006; Dowling and Wolff, 2023; Yan *et al.,* 2021). Pape (2001) analyzed the phylogeny of Oestridae at the genus level based on 118 morphological, physiological, ontological, and behavioral characteristics, establishing that four branches are divided into subfamily levels (Cuterebrinae, Gasterophilinae, and Hypodermatinae+Oestrinae). Here in the provided experiment, the evolutionary assessment of mt genome sequences revealed two primary clades separating the phylogenetic history of Oestroidea. Following the current research, the first clade consisted of nine species from Gasterophilinae, and the second one consisted of 41 species from 12 different dissimilar subfamilies. Moreover, although Cuterebrinae, Hypodermatinae, Oestrinae, and Gasterophilinae fall within Oestridae, in this evolutionary study, Gasterophilinae and other subfamilies did not show up in the same branch. These findings imply that more study is needed on the interactions between Oestridae and other families.

The first full mt genome of *H. sinense* presented in this work provides molecular understanding of the evolutionary links among Oestridae. We rebuilt the evolutionary tree of Oestridae and defined the family phylogenetic relationship between *H. sinense* and several Oestroidea larvae, so improving our knowledge of the general phylogenetic relationships within Oestroidea.

Conclusions: Finally, this work offers the first whole mitochondrial genome of *Hypoderma sinense*, thereby offering useful molecular information for knowledge of the evolutionary links within the Oestridae family. Through morphological and genomic analysis of *H. sinense*, species identification is improved, and the phylogenetic position of this parasite among related species is revealed. These results help to clarify parasite illnesses in cattle and promote the creation of more successful management and preventive plans.

Acknowledgments: The authors extend their appreciation to the Deanship of Research and Graduate Studies of King Khalid University for funding this work through a large group research project under a grant number (R.G.P. 2/7/45).

Competing interests: All the authors declare no conflict of interest.

Funding: West Tibet Autonomous Region Science and Technology Plan Project (XZ202401JD0012); West Tibet Autonomous Region Science and Technology Plan Project (XZ202401ZY0052); National Key Laboratory Open Project (XZNKY-CZ-2022-016-08).

Authors contribution: Conceptualization was from KL and WB, and methodology was designed by BS, XLZ, WQT, FBG, YBL, KL, QXW, and YC. The software was implemented by FQH, validation was done by KL, MA and QXW, formal analysis was performed by BS, DQ, MQ, MZZ, XYL, MA, , resources were managed by KL and QXW, data curation was conducted by BS, MA, AAE, AAG, KL and QXW, writing—original draft preparation was performed by BS, XLZ, WQT, FBG, YBL, MA, and KL, writing—review and editing was done by BS, FQH, DQ, MQ, MZZ, MA, AAE, AAG, KL and QXW, visualization by KL and QXW supervised by KL and QXW, project administration was conducted by KL, QXW, funding acquisition was by AAE, AAG and QXW. All authors have read and agreed to the published version of the manuscript.

REFERENCES

Ahmed H, Simsek S, Saki CE, *et al*., 2017a. Molecular characterization of *Hypoderma* spp. in domestic ruminants from Turkey and Pakistan. J Parasitol 103: 303–308.

Ahmed H, Sousa SR, Simsek S, *et al*., 2017b. First molecular characterization of *Hypoderma actaeon* in cattle and red deer (*Cervus elaphus*) in Portugal. Korean J Parasitol 55: 653–658.

Altschul SF, Gish W, Miller W, *et al*., 1990. Basic local alignment search tool. J Mol Biol 215: 403–410.

Bankevich A, Nurk S, Antipov D, *et al*., 2012. SPAdes: A new genome assembly algorithm and its applications to single-cell sequencing. J Comput Biol 19: 455–477.

Bentler PM, 2010. SEM with simplicity and accuracy. J Consum Psychol 20: 215–220.

Bernhardt V, Finkelmeier F, Verhoff MA, *et al*., 2019. Myiasis in humans—a global case report evaluation and literature analysis. Parasitol Res 118: 389–397.

Bernt M, Donath A, Jühling F, *et al*., 2013. MITOS: Improved de novo metazoan mitochondrial genome annotation. Mol Phylogenet Evol 69: 313–319.

Boore JL, 1999. Animal mitochondrial genomes. Nucleic Acids Res 27: 1767–1780.

Cameron SL, 2014. Insect mitochondrial genomics: implications for evolution and phylogeny. Annu Rev Entomol 59: 95–117.

Chen W, Zhang H, Meng R, *et al*., 2024. Genome-wide phylogenetic and genetic evolutionary analyses of mitochondria in *Hypoderma bovis* and *H. sinense* on the Qinghai-Tibetan Plateau. Parasitol Res 123(1): 43.

Chernomor O, Von Haeseler A, Minh BQ, 2016. Terrace aware data structure for phylogenomic inference from supermatrices. Syst Biol 65: 997–1008.

Coil D, Jospin G and Darling AE, 2014. A5-miseq: an updated pipeline to assemble microbial genomes from Illumina MiSeq data. Bioinformatics 31: 587–589.

Colwell DD and Otranto D, *et al*., 2021. Oestrid myiasis at a cross-road. Act Trop 224: 106131.

De Azeredo-Espin AML and Lessinger AC, 2006. Genetic approaches for studying myiasis-causing flies: molecular markers and mitochondrial genomics. Genetica 126: 111–131.

Dowling DK and Wolff JN, 2023. Evolutionary genetics of the mitochondrial genome: insights from *Drosophila*. Genetics 224.

González S, Del Rio ML, Diez MN, *et al*., 2023. Identification of *Hypoderma actaeon* (Diptera: Oestridae) in red deer (*Cervus elaphus*) from northern Spain: microscopy study and molecular analysis. Micros Res and Tech 86: 3–11.

González S, Panadero R, Del Rio ML, *et al*., 2024. Assesment of *Hypoderma* infestation in a wild population of *Cervus elaphus* from mountains Atlantic ecosystems in southwestern Europe (Spain). Vet Res Comm 48: 761–771.

Grant JR and Stothard P, 2008. The CGView Server: a comparative genomics tool for circular genomes. Nucleic Acids Res 36: 181–184.

Katoh K and Standley DM, 2016. A simple method to control over-alignment in the MAFFT multiple sequence alignment program. Bioinformatics 32: 1933–1942.

Kettle DS and Utsi MNP, 1955. *Hypoderma diana* (Diptera, Oestridae) and *Lipoptena cervi* (Diptera, Hippoboscidae) as parasites of reindeer (*Rangifer tarandus*) in Scotland with notes on the second-stage larva of *Hypoderma diana*. Parasitol 45: 116–120.

Kurtz S, Phillippy A, Delcher AL, *et al*., 2004. Versatile and open software for comparing large genomes. Genome Biol 5(2):R12.

Lanfear R, Frandsen PB, Wright AM, *et al*., 2017. PartitionFinder 2: New methods for selecting partitioned models of evolution for molecular and morphological phylogenetic analyses. Mol Biol Evol 34(3): 772-773.

Lessinger AC, Martins Junqueira AC, Lemos TA, *et al*., 2000. The mitochondrial genome of the primary screwworm fly *Cochliomyia hominivorax* (Diptera: Calliphoridae). Insect Mol Biol 9: 521–529.

Letunic I and Bork P, 2021. Interactive Tree Of Life (iTOL) v5: an online tool for phylogenetic tree display and annotation. Nucleic Acids Res 49: 293–296.

Li X, Pape T and Zhang D, 2019. *Gasterophilus flavipes* (Oestridae: Gasterophilinae): A horse stomach bot fly brought back from oblivion with morphological and molecular evidence. PLoS One 14: 220820.

Li X, Yan L, Pape T, *et al*., 2020. Evolutionary insights into bot flies (Insecta: Diptera: Oestridae) from comparative analysis of the mitochondrial genomes. Int J Biol Macromol 149: 371–380.

Li Xiuping, Zhang X, Jian Y, *et al*., 2020. Detection of *Cryptosporidium* oocysts and *Giardia* cysts in vegetables from street markets from the Qinghai Tibetan Plateau Area in China. Parasitol Res 119: 1847–1855.

Nguyen LT, Schmidt HA, Von Haeseler A, *et al*., 2015. IQ-TREE: A fast and effective stochastic algorithm for estimating maximum-likelihood phylogenies. Mol Biol Evol 32: 268–274.

Okonechnikov K, Golosova O and Fursov M, 2012. Unipro UGENE: a unified bioinformatics toolkit. Bioinformatics 28: 1166–1167.

Otranto D, Colwell DD and Pape T, 2005. *Hypoderma sinense*: solving a century-old enigma. Med Vet Entomol 19: 315–321.

Otranto D, Colwell DD, Traversa, D, *et al*., 2003. Species identification of *Hypoderma* affecting domestic and wild ruminants by morphological and molecular characterization. Med Vet Entomol 17: 316–325.

Otranto D, Johnson G, Syvrud K, *et al*., 2016. Treatment and control of bovine hypodermosis with ivermectin long-acting injection (IVOMEC® GOLD). Parasit Vectors 9: 1–6.

Otranto D, Paradies P, Testini G, *et al*., 2006. First description of the endogenous life cycle of *Hypoderma sinense* affecting yaks and cattle in China. Med Vet Entomol 20: 325–328.

Otranto D, Traversa D, Colwell DD, *et al*., 2004. A third species of *Hypoderma* (diptera: oestridae) affecting cattle and yaks in china: molecular and morphological evidence. J Parasitol 90: 958–965.

Pape T, 2001. Phylogeny of Oestridae (Insecta: Diptera). Syst Entomol 26: 133–171.

Patra G, Behera P, Das SK, *et al*., 2018. Bovine hypodermosis- A review. Int J Adv Agric Res 6: 18–29.

Rakhshandehroo E, Razavi SM, Farzaneh R, *et al*., 2019. Phylogenetic analysis of goat warble fly (*Przhevalskiana silenus*) based on mitochondrial COI gene. J Parasit Dis 43: 304–307.

Ronquist F, Teslenko M, Van der Mark P, *et al*., 2012. MrBayes 3.2: Efficient bayesian phylogenetic inference and model choice across a large model space. Syst Biol 61: 539–542.

Ruan W, Feng Y, Zhang L, *et al*., 2014. Health problems associated with international travel: a case of cutaneous myiasis in China due to *Cordylobia anthropophaga* imported from Uganda. Biosci Trends 8: 346–349.

Schubert M, Lindgreen S and Orlando L, 2016. AdapterRemoval v2: rapid adapter trimming, identification, and read merging. BMC Res Notes 9: 88.

Shaalan MG, Farghaly S, Khater EI, *et al*., 2024. Molecular characterization of the camel nasal botfly, *Cephalopina titillator* (Diptera: Oestridae). Beni-Suef Univ J Basic Appl Sci 131: 8.

Sunny B, Sulthana L, James A, *et al*., 2016. Maggot infestation: various treatment modalities. J Am Coll Clin Wound Spec 8: 51–53.

Talavera G and Castresana J, 2007. Improvement of phylogenies after removing divergent and ambiguously aligned blocks from protein sequence alignments. Syst Biol 56: 564–577.

Walker BJ, Abeel T, Shea T, *et al*., 2014. Pilon: An integrated tool for comprehensive microbial variant detection and genome assembly improvement. PLoS One 9: 112963.

Wang H-C, Minh BQ, Susko E, *et al*., 2018. Modeling site heterogeneity with posterior mean site frequency profiles accelerates accurate phylogenomic estimation. Syst Biol 67: 216–235.

Weigl S, Testini G, Parisi A, *et al*., 2010a. The mitochondrial genome of the common cattle grub, *Hypoderma lineatum*. Med Vet Entomol 24: 329–335.

Weigl S, Traversa D, Testini G, *et al*., 2010b. Analysis of a mitochondrial noncoding region for the identification of the most diffused *Hypoderma* species (Diptera, Oestridae). Vet Parasitol 173: 317–323.

Yan L, Xu W, Zhang D, *et al*., 2021. Comparative analysis of the mitochondrial genomes of flesh flies and their evolutionary implication. Int J Biol Macromol 174: 385–391.

Zhang D, Gao F, Jakovlić I, *et al*., 2020. PhyloSuite: An integrated and scalable desktop platform for streamlined molecular sequence data management and evolutionary phylogenetics studies. Mol Ecol Resour 20: 348–355.

Zhang F, Zhang H, Li Z, *et al*., 2025. Evolutionary analysis of *Hypoderma pantholopsum* in Tibetan antelopes on the Qinghai–Tibetan Plateau. Act Para 70(1): 9.